frontiers | Frontiers in Materials

TYPE Original Research
PUBLISHED 11 August 2022
DOI 10.3389/fmats.2022.980907

OPEN ACCESS

EDITED BY
Weifu Sun,
Beijing Institute of Technology, China

REVIEWED BY
Yongzhi Cheng,
Wuhan University of Science and Technology, China
Jiafu Wang,
Air Force Engineering University, China

*CORRESPONDENCE
Liuying Wang,
lywangxa@163.com

SPECIALTY SECTION
This article was submitted to Metamaterials, a section of the journal Frontiers in Materials

RECEIVED 29 June 2022
ACCEPTED 11 July 2022
PUBLISHED 11 August 2022

CITATION
Chen M, Wang L, Liu G, Ge C, Wang L, Xu K and Wang W (2022), Structural design and optimization of double-cross shape broadband absorption metamaterial based on CB-ABS. *Front. Mater.* 9:980907. doi: 10.3389/fmats.2022.980907

Structural design and optimization of double-cross shape broadband absorption metamaterial based on CB-ABS

Mengzhou Chen, Liuying Wang*, Gu Liu, Chaoqun Ge, Long Wang, Kejun Xu and Weichao Wang

Xi'an Research Institute of High Technology, Xi'an, China

This work presents a novel broadband double-cross shape metamaterial structure based on the Carbon Black-Acrylonitrile-Butadiene-Styrene (CB-ABS) composite material. The optimal metamaterial structure with the thickness of 7 mm shows a broadband absorption characteristic in the frequency range of 5.1–40 GHz. Additionally, the low volume filling fraction of the proposed metamaterial structure will be helpful to achieve lightweight broadband absorption performance. Meanwhile, the metamaterial structure can also display a wide-angle absorption performance from 0° to 55° for TE mode and 0°–75° for TM mode. Moreover, this research provides an effective and promising way for the practical application of the lightweight broadband and wide-angle microwave strong absorption metamaterial in the future.

KEYWORDS

metamaterial structure, electromagnetic properties, broadband absorption, double-cross shape, polarization and angle independence

Introduction

Electromagnetic metamaterials have received extensive attention from researchers due to their tunable electromagnetic properties (Fu et al., 2019; Wang et al., 2020). Different from traditional materials, the unique electromagnetic properties of metamaterials are mainly derived from the periodic structural units and the variation in arrangement (Chen et al., 2022; Liu et al., 2021; Mei et al., 2019; Xiong et al., 2022; Zhang et al., 2020a). However, the single-frequency absorption characteristic of traditional absorbing metamaterials limits their application field (Landy et al., 2008). While expanding the spectral compatibility of traditional absorbing material by introducing metamaterials has become a hot research direction in the electromagnetic wave absorption field (Duan et al., 2020; Hu et al., 2021; Pang et al., 2018; Xu et al., 2017; Zhang et al., 2020b). Up to now, researchers have proposed several ways to obtain the broadband absorption characteristic, including loading lumped elements (Li et al., 2019; Liu et al., 2021; Wang and Chen, 2020; Zhang et al., 2021a), multi-layer structure stacking (Yang et al., 2020; Zhou et al., 2017a), and unit structure resonance interference (Chen, 2012; Cheng et al., 2020; Costa et al., 2012; Duan et al., 2021; Sheng et al., 2019; Song et al.,

2019). However, the conductive loss of metal components and the polarization and angle sensitivity of the planar structure in these methods also seriously impede their engineering application.

Meanwhile, carbon-based materials like conductive carbon black, carbon nanotubes, and graphene composites are crucial in the development of lightweight broadband absorbing metamaterials (Chen et al., 2020; Jing et al., 2021; Lei et al., 2020; Luo et al., 2022; Luo et al., 2022; Mei et al., 2021,2019). Compared with magnetic materials, carbon-based materials have the ability to absorb electromagnetic waves with lower density, making it easier to meet lightweight and broadband design requirements. Under the premise of meeting the specified size and surface quality, 3D printing components prepared with engineering plastics and resins such as (Polylactic Acid, PLA) and (Acrylonitrile-Butadiene-Styrene composites, ABS) can have good machining performance and light weight (Dong et al., 2020; Duan et al., 2021; Kotsilkova et al., 2017; Shen et al., 2018). And since graphene has good dielectric loss properties, Yin et al. (2019) used reduced graphene oxide (RGO) as the absorbent, while PLA as the matrix to prepare composite metamaterials with a gradient index of impedance (GRIN). Using ABS as the matrix material, Ren and Yin (2018) successfully effectively fabricated the metamaterial structure with the effective bandwidth covering the C and X band. The metamaterial structure is composed of an array of cylindrical dielectric resonators. By exciting the different working modes of the resonator, ultra-broad effective band is available. A lot of researchers have become attracted in resin materials due to their low density, good thermal stability, and superior comprehensive properties. Xiao et al. (2019) fabricated SiC nanowire/acrylic resin (SiC_{nw}/ACR) composites with broadband electromagnetic absorption capabilities using 3D stereolithography printing technology, and enhanced the composites by adjusting the content of SiC_{nw} and the thickness of the printed layer. Huang et al. (2020) prepared a periodic hollow truncated cone structure with photosensitive resin. The surface layer of the structure was coated with conductive carbon pasted by the impregnation method. The synergistic effect of structure and material properties significantly enhanced the broadband electromagnetic wave absorption properties.

In this paper, we proposed a double-cross shape metamaterial structure based on the Carbon Black-Acrylonitrile-Butadiene-Styrene (CB-ABS) composite material. The designed metamaterial structure was demonstrated to show an ultra-broadband absorption in the frequency of 5.1–40 GHz. In order to investigate the mechanism of broadband absorption, the electromagnetic field distribution and power loss density at the absorption peaks were analyzed. Respectively, the polarization insensitivity and oblique incident characteristics under TE and TM modes were calculated and analyzed by numerical simulation. Furthermore, as the metamaterial structure is relatively simple, the difficulty of fabrication and realization is greatly reduced, which will greatly accelerate its practical application.

Experimental section

Structure design and simulation

Figure 1 depicts a schematic diagram of the proposed metamaterial structure, which represents different views. To enhance the angular and polarization stability of the metamaterial structure, a 45° rotation cross grating is added to the conventional decagonal cell. Then we combine the double-cross shape and flat structure to improve the broadband absorption performance. The double-cross shape structure is formed by the rotation and combination of cuboids. And the length, width, and height of the cuboid are W, L and H_2, correspondingly. The thickness of the bottom flat structure was set as H_1, and the side length was L. The optimal structural parameters obtained through theoretical simulation and scanning optimization are L = 26 mm, H_1 = 2 mm, H_2 = 5 mm, and W = 3 mm.

In this paper, the metamaterial structure was designed and analyzed by the commercial software CST Microwave Studio through the Finite Integration Technique (FIT) calculation principle. In CST, a linearly polarized planar wide-spectrum wave incidence on the metamaterial surface is used for simulation. The wave vector is along the z-axis, the direction of electric field vector is parallel to y-axis, and the direction of magnetic field vector is parallel to x -axis. The Floquet modes are used to generate and receive the transverse TE and TM mode waves that incident on the metamaterial structure along the z-axis. The unit cell boundary conditions are set in the *x* and *y* directions to simulate an infinitely periodic array of metamaterial structure, while that along the z direction is open add space. The absorption can be calculated as:

$$A(w) = 1 - R(w) - \boldsymbol{T}(w) = 1 - |S_{11}(w)|^2 - |S_{22}(w)|^2 \quad (1)$$

where $\boldsymbol{R}(\boldsymbol{w})$ and $\boldsymbol{T}(\boldsymbol{w})$ are the reflection and transmission, respectively. Since the bottom metal plate of the proposed metamaterial structure prevents the transmission of electromagnetic waves, the absorption of electromagnetic waves can be simplified to

$$\boldsymbol{A}(\boldsymbol{\omega}) = 1 - |S_{11}(\boldsymbol{\omega})|^2 \quad (2)$$

Materials, fabrication, and measurement

The microwave loss material carbon black (CB), as shown in Figure 2A, was purchased from Suzhou First Element Nanotechnology Co., in China. The Acrylonitrile-Butadiene-Styrene (ABS) polymer powder was supplied by Dongguan Jiecheng Technology Co. in China, which serves as the thermoplastic matrix. To prepare the CB-ABS composite filaments, the CB and ABS powder were firstly dried in the drying oven at 80°C for 8 h. Then, the mixture with the mass

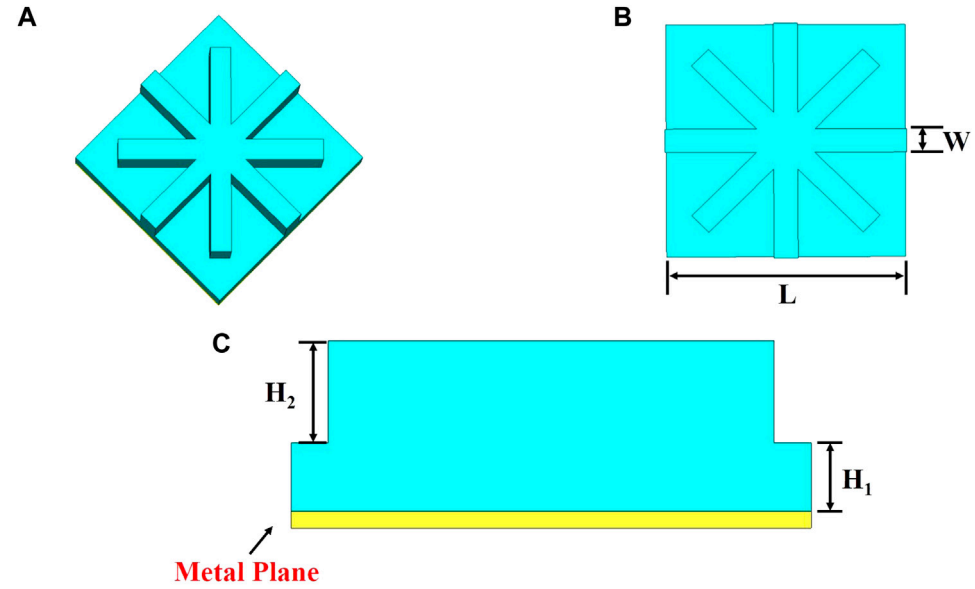

FIGURE 1
(A) Schematic diagram of unit cells; the top view **(B)** and sectional view **(C)** of unit cells.

ratio of CB/ABS being 1:7 was dispersed in the planetary mixer at 60 r/min for 5 h. Finally, the uniformly dispersed powder mixture was poured into the single-screw extruder to fabricate the 1.75 ± 0.1 mm composite filaments under 230°C. The sample for electromagnetic parameters and reflectivity measurement was fabricated via the FDM 3D printing machine (3D Raised E2, China). A vector network analyzer (Ceyear 3672C, China) was used to measure the complex permittivity and permeability of the CB- ABS composite filaments at 2–18 GHz using the coaxial line method.

Results and discussion

Electromagnetic properties of the composite filaments

The permittivity and permeability of CB-ABS composite filaments in the range of 2–18 GHz are shown in Figure 2A. Both the real and imaginary parts of the permittivity decrease continuously with the increase of frequency, while the change of the imaginary part is relatively slight. However, both the real and imaginary parts of the permeability are basically unchanged. Figure 2B shows the reflectivity variation curves of the single-layer flat composite versus frequency with different thicknesses. The calculation result shows that the lower boundary of the effective absorption bandwidth continuously moves towards the lower frequency with the thickness increasing from 2 to 7 mm. And broadband electromagnetic wave absorption cannot be achieved through the single-layer flat structure. The electromagnetic loss of the CB-ABS composite material is mainly the dielectric loss, and the multiple reflection originates from the gap formed by the absorbent and the matrix.

According to the quarter-wavelength matching mechanism, the matching thickness (d_m) of the absorbing material and its corresponding absorption peak frequency (f_m) satisfy the following equation (Q. Zhou et al., 2017b):

$$d_m = \frac{n\lambda}{4} = \frac{nc}{4f_m\sqrt{|\mu||\varepsilon|}} (n = 1, 3, 5 \ldots) \quad (3)$$

where λ is the wavelength of the electromagnetic wave in the absorption material, while $|\varepsilon|$ and $|\mu|$ are the modulus values of the permittivity and permeability at the corresponding frequency, respectively. Figure 2C shows the RL curve of the single-layer CB-ABS absorption composites with different thicknesses. The change curve of d_m and f_m corresponding to CB-ABS calculated by the $\lambda/4$ matching model is shown in Figure 2D. The solid dots of different colors in Figure 2D are the matching thickness d_m and its corresponding absorption peak frequency f_m, which extracted from the RL curve with different thicknesses in Figure 2C. And they are basically located around the $\lambda/4$ curve, indicating that the absorption peak of the single-layer CB-ABS absorption composite material obeys the $\lambda/4$ model.

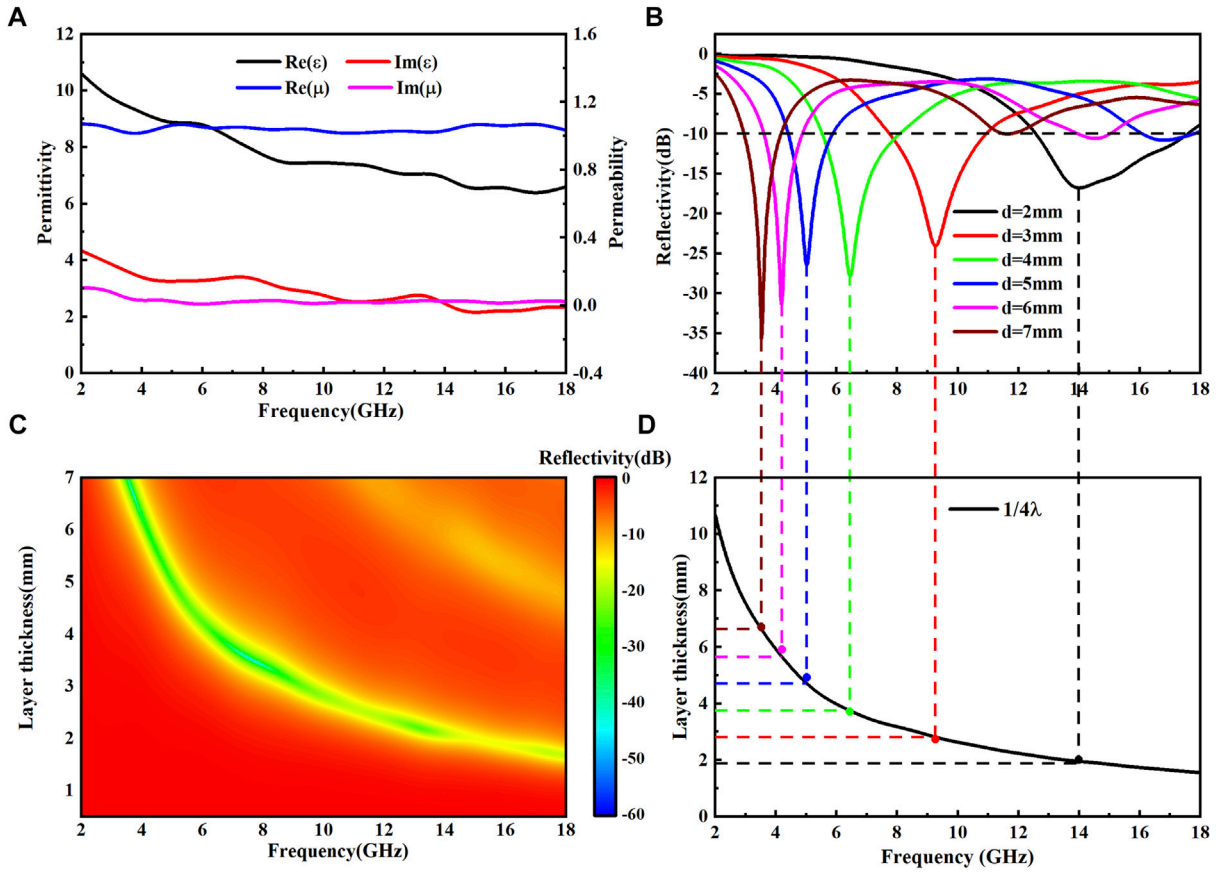

FIGURE 2
(A) The frequency dependence of permittivity and permeability for CB-ABS composite; **(B)**The distribution map of the RL curves for the single layer composites with thickness and frequency; **(C)** RL curves with different thicknesses; **(D)** calculated curve of thickness versus peak frequency under λ/4 model.

Optimization of structural parameters

The performance optimization of the double-cross shape metamaterial structure can be divided into the geometric parameters (L, W, and H) of double-cross shape and the shape of step surfaces.

Figure 3A depicts the effects of H_1 on the peak frequency shift and bandwidth of the reflectivity spectrum. Based on the change pattern of reflectivity under different thicknesses of the single-layer flat composite material, H_1 + H_2 is set as 7 mm. When varying H_1 from 1 to 6 mm with an interval of 1 mm, the thickness of the double-cross shape structure decreases. Simultaneously, the first reflectivity peak of the metamaterial structure moves towards the lower frequency. While the H_1 exceeds 2 mm, the reflectivity intensity around 10 GHz starts to decrease continuously. Considering the absorption performance in the frequency range of 2–40 GHz, H_1 = 2 mm and H_2 = 5 mm can be selected to achieve broadband absorption characteristics.

Figure 3B shows the RL curves of periodic double-cross shape metamaterial structure with different side length L. With the increasing L, the absorption performance of the metamaterial structure around 5 GHz gradually deteriorates, and the first reflectivity peak keeps moving to the higher microwave band, while the reflectivity intensity at the frequency peak gradually strengthens. Moreover, the variety of L has a great impact on the absorption strength and effective bandwidth of the medium and lower frequencies, while the influence on the higher frequency is slight.

Meanwhile, as shown in Figure 3C, it can be concluded that the influence of the width W and H_1 of the double-cross shape structure on lower frequency absorption performance is similar. And the reflectivity intensity at the first absorption peak is greatly improved when W increases from 1 to 3 mm. The reason for this phenomenon is that the increasing W improves the equivalent electromagnetic parameters when other structural parameters remain constant, and the equivalent electromagnetic parameters play an important role in the material loss capability. At the same time, the space between the branches of the double-cross shape structure decreases with the

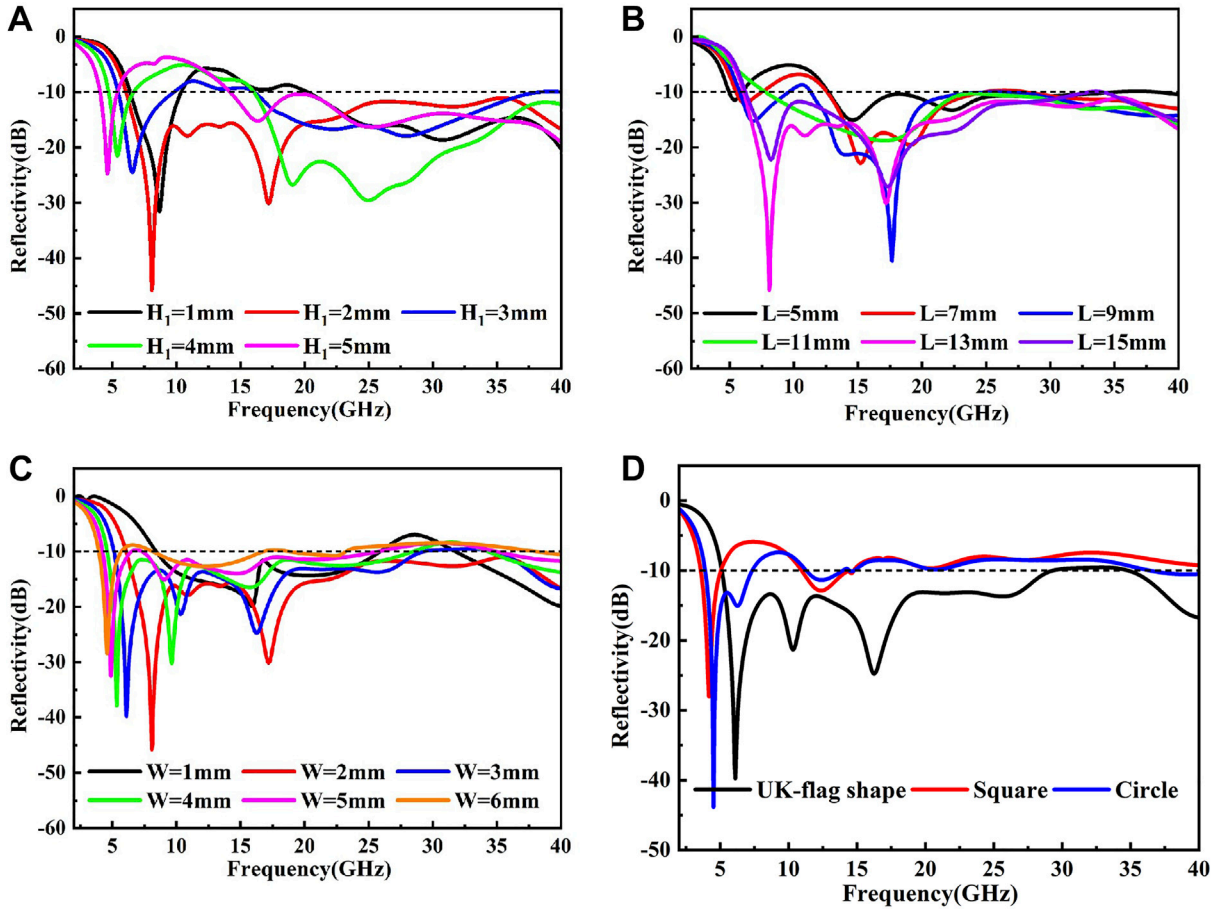

FIGURE 3
Influence of different structural parameters in the unit cell of **(A)** H_1; **(B)** L; **(C)** W, and **(D)** the surface shape on the reflectivity in the frequency range of 2–40 GHz.

increasing W from 1 to 2 mm, which enhances the structural resonance effect. However, the branches at all levels of the double-cross shape structure tend to overlap when W continues to increase, and the reflectivity intensity at medium and higher frequency positions continues to decrease. As a result, other loss mechanisms, such as resonance interference and edge diffraction, may be weakened. Integrating the effective bandwidth and absorption intensity in the whole frequency range of 2–40 GHz, the optimal structural parameters combination for the double-cross shape metamaterial structure is confirmed as H_1 = 2 mm, H_2 = 5 mm, W = 3 mm, and L = 26 mm.

Furthermore, the influence of surface shape of different unit structures is also discussed and analyzed in Figure 3D. Compared with square and circle shapes, the absorption performance of the double-cross shape metamaterial structure around 5 GHz is relatively poor with the same structural thickness and unit cell size. However, the double-cross shape structure has the widest absorption band width, and the highest reflectivity intensity in the whole frequency range. Therefore, the simulation result proves the rationality of the double-cross shape structure design. In addition to the above results, the volume filling fraction of different metamaterial structure shapes is calculated. Assuming that the volume filling fraction of a cuboid with the length, width, and height of 26, 26, and 7 mm is 1, the volume filling fractions T of the various unit structure shapes are as follows:

$$T_{double-cross} = \frac{L^2*H_1 + 4L*W*H_2 - 3W^2}{L*L*H} = 0.503 \quad (4)$$

$$T_{Circle} = \frac{L^2*H_1 + \pi*(L/2-1)^2*H_2}{L*L*H} = 0.847 \quad (5)$$

$$T_{Square} = \frac{L^2*H_1 + (L-2)^2*H_2}{L*L*H} = 0.797 \quad (6)$$

It can be concluded that the volume filling fractions of the metamaterial structure can be significantly reduced by the design

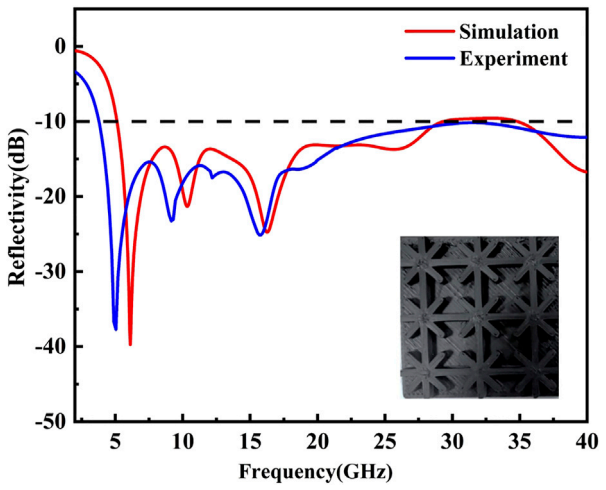

FIGURE 4
Comparison of the simulation and experimental reflectivity the double-cross shape metamaterial structure in the frequency range of 2–40 GHz.

of the double-cross shape structure under the same thickness. Furthermore, as the absorbent, CB has the advantage of light weight, and the density of the CB-ABS composite filament is only 0.27 g/cm^3. Therefore, the designed metamaterial structure can satisfy the requirements of light weight and broadband absorption through the lower volume filling fraction and density of composite filament (Fu et al., 2019).

Simulation and experimental results were also depicted and analyzed in Figure 4. The simulation effective bandwidth of the double-cross shape metamaterial structure can cover the frequency range of 5.1–40 GHz. For the experimental reflectivity, it can realize below −10 dB absorbing bandwidth from 3.9 to 40 GHz. It is indeed that the overall trend of simulated and experimental results agrees well. The differences between the measured and simulated results mainly originate from the manufacturing error and measurement limitation. Firstly, the differences may be induced by the surface quality and structural deformation during the fabricating process. In addition, due to the limitations of the test system, we measured reflectivity with an incident angle of 5° instead of the normal incidence angle. The comparison shows that the double-cross shape metamaterial structure is effective to achieve broadband microwave absorption.

As shown in Figure 5, the proposed metamaterial structure is clearly superior to other related works due to its relatively broad absorption performance and thin thickness. Compared with the metamaterial with dielectric loss material, the proposed metamaterial structure has a smaller thickness and more excellent absorbing properties. Even compared with the metamaterial containing magnetic material, such as the α Fe and carbonyl iron, it still has a similar absorption characteristic with the lower density. Meanwhile, the double-cross shape metamaterial structure in this work not only has excellent absorbing properties but also possesses a simple unit cell structure.

Polarization and angle independence

The polarization property of the metamaterial structure is analyzed by the numerical simulation. As shown in Figure 6, the electromagnetic wave is converted from TE mode to TM mode with the increasing polarization angle phi from 0° to 90°, while the electromagnetic wave absorption performance basically remains unchanged. This result is due to the strong rotational symmetry of the double-cross shape, which can overlap with itself after rotating 45°. Furthermore, the proposed structure is centrosymmetric. Therefore, the proposed metamaterial structure not only greatly improves the electromagnetic wave absorption properties of CB-ABS composite material but also makes the wave isotropic absorption properties.

The absorption properties of the oblique incident with different incident angles for TE polarization and TM polarization were also analyzed and the results are presented in Figures 7, 8. For TE polarization, the reflectivity intensity of the first absorption peak decreases gradually with the increasing incident angle. The reason is that the first absorption peak is related to the λ/4 magnetic resonance, and the resonance intensity decreases with increasing incidence angle. The reflectivity intensity of the absorption peak around 17.5 GHz decreases with the increase of the incident angle, as this absorption peak is mainly attributed to the resonance between adjacent unit cells and the branches of the double-cross shape of weak electric and strong magnetic resonance. Simultaneously, the reflectivity intensity in the frequency range of 20–40 GHz changes slightly within the incident angle of 0°–45°. While the incident angle exceeds 45°, the reflectivity intensity is higher than -10 dB in most frequency ranges.

For TM polarization, the change pattern of the reflectivity intensity of the first absorption peak is similar to that under the TE polarization. However, the position of this absorption peak has shifted to some extent. Furthermore, the reflectivity intensity around 17.5 GHz first increases and then decreases, which leads to a maximum absorption at 45°. According to the comprehensive analysis of absorption performance in the frequency range of 2–40 GHz, the double-cross shape metamaterial structure is less sensitive to the change of the incident angle under TM polarization than that under TE polarization. The effective bandwidth remains basically unchanged within the incident angle of 0°–60°, and even when the incident angle reaches 75°, the reflectivity intensity in the frequency range of 10–40 GHz is close to 90%.

As the absorbing properties of the metamaterial structure are mainly related to the magnetic field strength along the direction

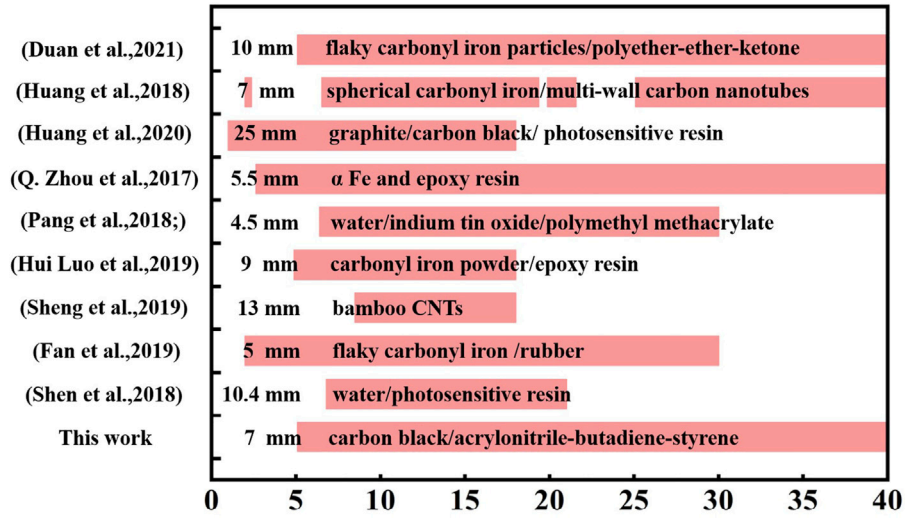

FIGURE 5
Comparison of −10 dB absorption bandwidth range between this work and previous works.

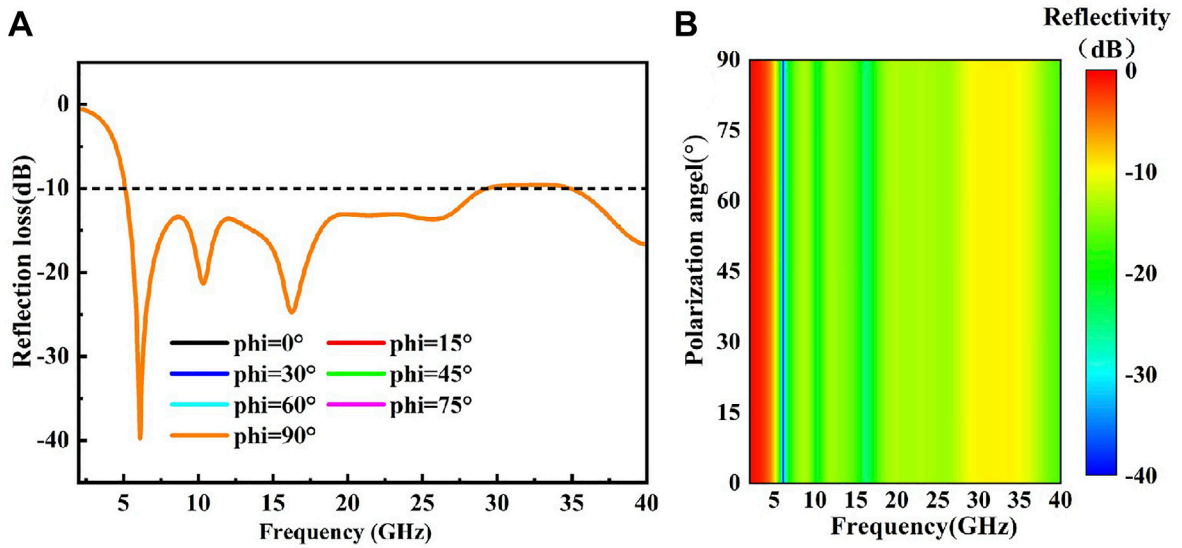

FIGURE 6
Polarization response spectrum of the incident electromagnetic wave: **(A)** Line diagram in specific angle; **(B)** Contour diagram.

of the metamaterial surface. When the incident angle gradually increases, the angle between the magnetic field direction of the TE mode electromagnetic wave and the surface of the metamaterial structure increases continuously, resulting in a continuous decrease of its magnetic field component and a weakening of the electromagnetic wave absorbing ability. With the increasing incident angle under the TM mode, the angle between the electric field direction and the surface of the metamaterial structure increases, while the direction and magnitude of the magnetic field component do not change. The fundamental reason is that the electric and magnetic fields of TE and TM waves no longer have symmetry under oblique incidence, and it is difficult for symmetric structures to produce the same response to asymmetric electromagnetic field. The difference in the response of the two polarization waves is even more obvious.

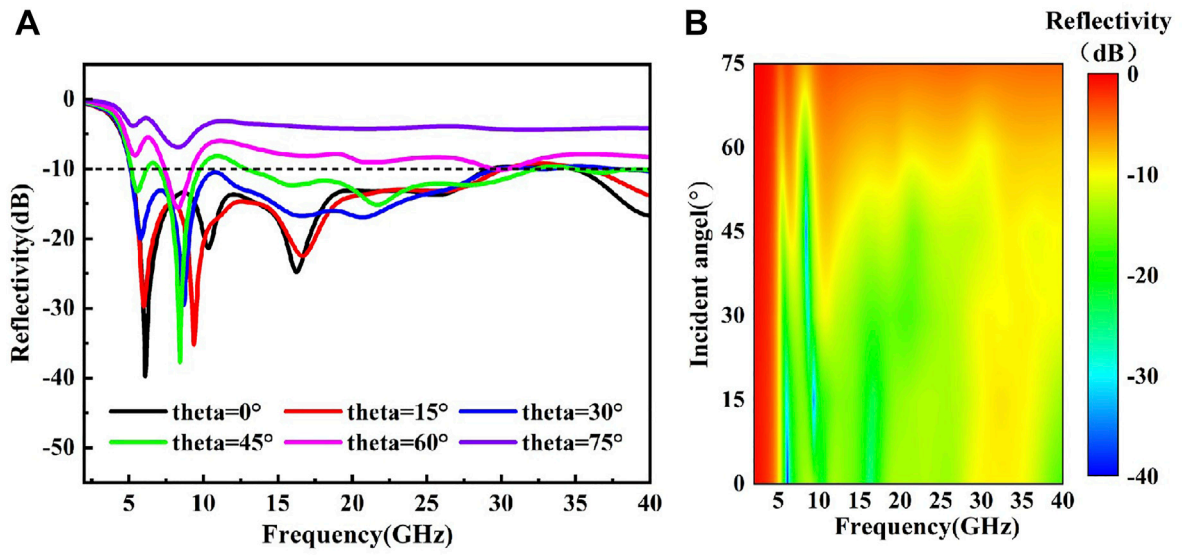

FIGURE 7
Oblique incident response spectra of the incident electromagnetic wave in TE mode: **(A)** Line diagram in specific angle; **(B)** Contour diagram.

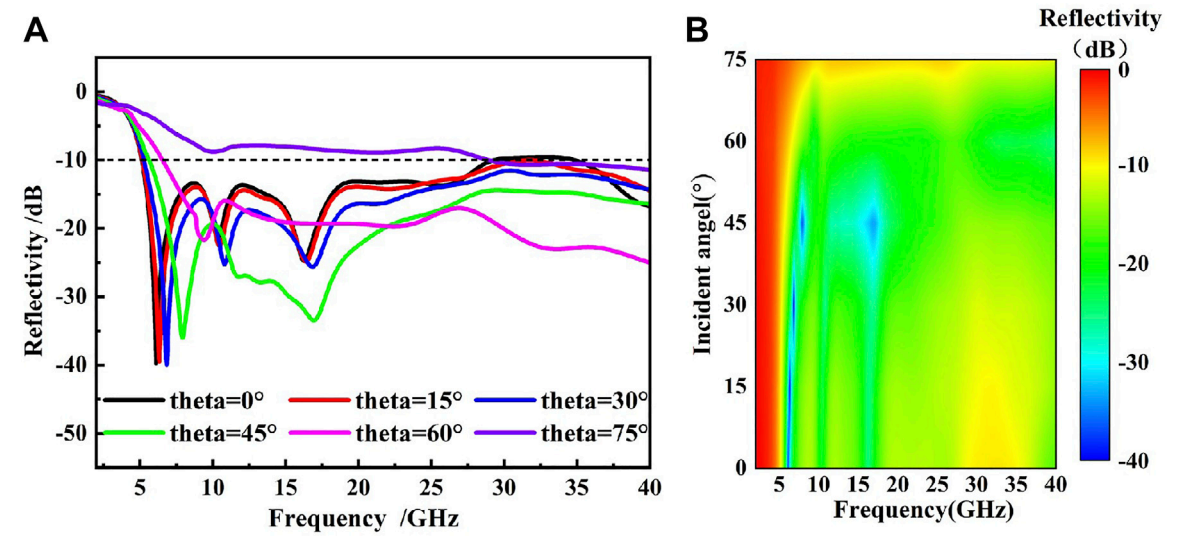

FIGURE 8
Oblique incident response spectra of the incident electromagnetic wave in TM mode: **(A)** Line diagram in specific angle; **(B)** Contour diagram.

We can conclude that the descending gradient of average absorptivity increases continuously with the increasing incident angle. The reason is that a large incident angle leads to the electromagnetic field component decreasing sharply. On the whole, the average absorptivity of the TM mode is better than TE mode at most angles. The reason is that under the same incident angle of TE and TM modes, the coupling lengths between electromagnetic field components and the proposed structure are different. Furthermore, the energy loss caused by the magnetic field is greater than that from the electric field at most angles, especially in the GHz band (C. Zhang et al., 2021b).

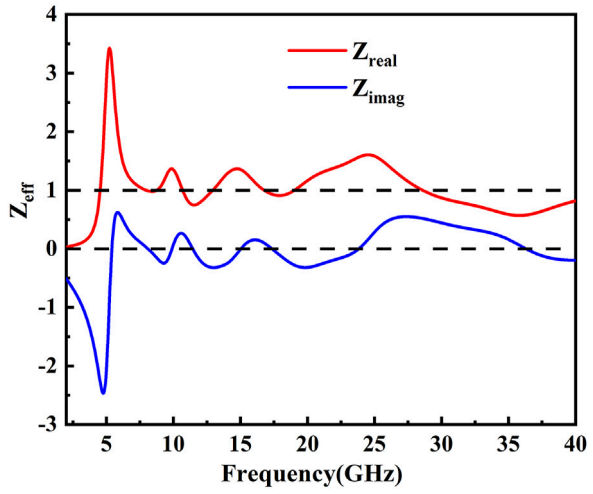

FIGURE 9
The effective input impedance of the double-cross shape metamaterial structure.

Analysis of broadband absorption mechanism

Impedance matching is a prerequisite for absorbing electromagnetic waves effectively. When the effective input impedance is matched to that of the air, the reflection will be minimized, and perfect absorption can be obtained. According to the following formula, the effective input impedance of the proposed metamaterial structure can be calculated (Hui Luo et al.):

$$Z_{eff} = \sqrt{\frac{\mu_{eff}}{\varepsilon_{eff}}} = \sqrt{\frac{(1+S_{11})^2 - S_{21}^2}{(1-S_{11})^2 - S_{21}^2}} \tag{7}$$

where ε_{eff} and μ_{eff} are the effective permittivity and permeability, S_{11} and S_{21} are the reflection and transmission parameters, respectively. The effective input impedance of the proposed metamaterial structure is generated by the combination of the periodic structure composite material with the metal grounded plate. Furthermore, due to the metamaterial structure is backed by a metallic plate, $S_{21} = 0$. As shown in Figure 9, the real and imaginary parts of Z_{eff} are calculated through S parameters. It is found that the real part of Z_{eff} in the frequency range of 6.1–40 GHz is close to 1, while the imaginary part of is nearly 0. And the trend of Z_{eff} versus frequency is fairly consistent with the reflectivity curve. This result indicates that the proposed metamaterial structure has a good impedance matching characteristic over a wide frequency range. The excellent impedance matching characteristic enables the majority of the electromagnetic wave can enter the interior of the structure and so that it can be effectively attenuated. Therefore, the proposed metamaterial structure has excellent broadband absorption.

The electric and magnetic field intensity distributions were further simulated and analyzed at four absorption frequencies of 6.1, 10.4, 16.3, and 40 GHz, respectively. As shown in Figure 10A, at the first lower absorption peak of 6.1 GHz, the electric field is mainly distributed in the upper part of the adjacent unit cell and the space above the metamaterial structure in the x-z plane. Compared with the electric field, the magnetic field mainly concentrates on the central position of the unit cell, including the central of the bottom layer and the double-cross shape structure. As for the power loss, it concentrates on the central location of the double-cross shape structure, which is more similar to the magnetic field distribution. This result reveals that the major power loss at 6.1 GHz is mainly derived from $\lambda/4$ magnetic resonance (Huang et al., 2018).

As the frequency increases to 10.4 GHz, the electric and magnetic field distributions are shown in Figure 10B. The electric field distribution shifts to the middle location of the double-cross shape layer and the top position of the branch structure in the x-z plane. Compared with the magnetic field distribution at 6.1 GHz, there is a slight enhancement at the void position of the unit cell in the y-z plane, which shows a weak resonance of adjacent unit cells. While the magnetic field of the double-cross shape layer decreases to some extent. The power loss at 10.4 GHz shown in Figure 10B concentrates on the edges of the top positions of branch structures and the void location of adjacent unit cells. This result indicates the power loss at 10.4 GHz is mainly attributed to strong resonance between adjacent unit cells and weak edge diffractions (Duan et al., 2021; Luo et al., 2019).

With the increasing frequency, as shown in Figure 10C, centering at 16.3 GHz, the electric field energy enhances further in the air gap between adjacent unit cells, while the electric field distribution on the edge of the branch structure weakens significantly. Additionally, the magnetic field distribution moves towards the junction of the branch structure, where the magnetic field and electric field concentration areas begin to overlap. As for the power loss, which is mainly distributed on the top and side edges of the double-cross shape metamaterial structure. It reveals that the power loss at 16.3 GHz mainly originates from the resonance between adjacent unit cells and weak edge diffractions (Fan et al., 2019).

Meanwhile, Figure 10D depicts the electric field, magnetic field, and power loss distributions at the highest frequency of 40 GHz. We can easily discover that there exists an intense distortion in the electric field and magnetic field distribution. Additionally, the electric field energy generated by the resonance between adjacent unit cells declines severely, while that at the edge of the top surface of the metamaterial structure enhances slightly. In general, compared with 16.3 GHz, the magnetic field energy distribution significantly. The magnetic field mainly concentrates on the top surface of the unit cell, especially, the edge area of the branches. The concentration of power loss on the edges of the top surface is similar to the

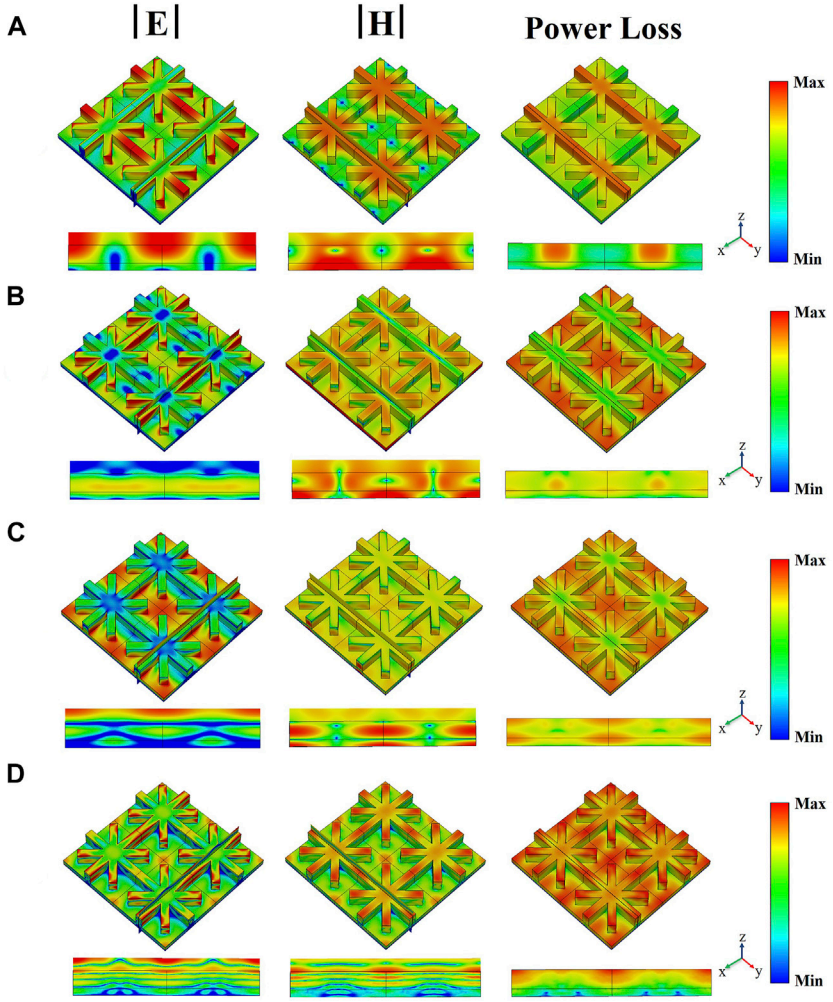

FIGURE 10
Distributions of the electric field, magnetic field and power loss of the double-cross shape metamaterial structure at four different frequency positions: **(A)** 6.1 GHz; **(B)** 10.4 GHz; **(C)** 16.3 GHz; **(D)** 40 GHz.

electric field and magnetic field. Moreover, from the analysis of the cross-sectional view of energy loss, it can be concluded that the concentration of power loss on the edges of the top surface is significantly stronger than that at the center location, which indicates the power loss of 40 GHz mainly results from the strong edge diffraction.

In conclusion, through the analysis of the effective input impedance, electromagnetic field and power loss distributions, it can be concluded that the double-cross shape metamaterial structure based on CB-ABS composite material can maintain an excellent impedance matching characteristic in a broadband frequency range, and the microwave absorption is attributed to λ/4 magnetic resonance, resonance between the branches of the double-cross shape structure and the adjacent unit cells, and edge diffraction on the edges of the top surface.

Conclusion

In summary, a double-cross shape metamaterial structure based on CB-ABS composite material was proposed to show an ultra-broadband absorption characteristic, which results from the combination of the material loss and novel structural design. Through the optimization function, the proposed metamaterial structure can basically realize the effective absorption in the frequency range of 5.1–40 GHz. Meanwhile, the volume filling fraction of different metamaterial structure shapes was calculated and compared, while the result indicates the double-cross shape has the smallest weight and satisfies the lightweight and broadband absorption requirements. The proposed metamaterial structure has excellent polarization independence properties, and it can maintain the broadband absorption within the oblique incident angle from 0 to 45° for TE

polarization and 0–75° for TM polarization. Furthermore, the effective input impedance of the proposed metamaterial structure was calculated and analyzed through the S parameters, which matches that of the free space in a wide frequency range. Finally, according to the analysis of electromagnetic field and energy loss distribution, the electromagnetic wave energy is mainly dissipated by the λ/4 resonances in the lower frequency, resonances between adjacent unit cells in the middle frequency range, and edge diffraction effects in the higher frequency range. It is believed that this research could provide a new strategy for the engineering application of the lightweight broadband metamaterial structure in the future.

Data availability statement

The original contributions presented in the study are included in the article/Supplementary Material, further inquiries can be directed to the corresponding author.

Author contributions

MC, LW, and GL contributed to conception and design of the study. MC organized the database. CG performed the statistical analysis. MC wrote the first draft of the manuscript. MC, KX, and WW wrote sections of the manuscript. All authors contributed to manuscript revision, read, and approved the submitted version.

Funding

This work was supported by the Natural Science Foundation of Shaanxi Province of China (No. 2022JQ-356) and the Youth Fund of Rocket Force University of Engineering (No. 2022QN-B017).

Conflict of interest

The authors declare that the research was conducted in the absence of any commercial or financial relationships that could be construed as a potential conflict of interest.

Publisher's note

All claims expressed in this article are solely those of the authors and do not necessarily represent those of their affiliated organizations, or those of the publisher, the editors and the reviewers. Any product that may be evaluated in this article, or claim that may be made by its manufacturer, is not guaranteed or endorsed by the publisher.

References

Chen, F., Zhang, S., Ma, B., Xiong, Y., Luo, H., Cheng, Y., et al. (2022). Bimetallic CoFe-MOF@Ti3C2Tx MXene derived composites for broadband microwave absorption. *Chem. Eng. J.* 431, 134007. doi:10.1016/j.cej.2021.134007

Chen, H. (2012). Interference theory of metamaterial perfect absorbers. *Opt. Express* 20 (7), 7165. doi:10.1364/OE.20.007165

Chen, X., Wu, Z., Zhang, Z., and Zou, Y. (2020). Graphene oxide aqueous solution-based metamaterial for broadband absorption. *Phys. E Low-dimensional Syst. Nanostructures* 120, 114017. doi:10.1016/j.physe.2020.114017

Cheng, Y., Luo, H., and Chen, F. (2020). Broadband metamaterial microwave absorber based on asymmetric sectional resonator structures. *J. Appl. Phys.* 127 (21), 214902. doi:10.1063/5.0002931

Costa, F., Monorchio, A., and Manara, G. (2012). Efficient analysis of Frequency-Selective surfaces by a simple Equivalent-Circuit model. *IEEE* 54, 35-48. doi:10.1109/MAP.2012.6309153

Dong, J., Huang, X., Muley, P., Wu, T., Barekati-Goudarzi, M., Tang, Z., et al. (2020). Carbonized cellulose nanofibers as dielectric heat sources for microwave annealing 3D printed PLA composite. *Compos. Part B Eng.* 184, 107640. doi:10.1016/j.compositesb.2019.107640

Duan, B., Zhang, J., Wang, P., Wang, G., He, D., Qiao, L., et al. (2020). Design and preparation of an ultrathin broadband metamaterial absorber with a magnetic substrate based on genetic algorithm. *J. Magn. Magn. Mat.* 501, 166439. doi:10.1016/j.jmmm.2020.166439

Duan, Y., Liang, Q., Yang, Z., Li, Z., Yin, H., Cao, Y., et al. (2021). A wide-angle broadband electromagnetic absorbing metastructure using 3D printing technology. *Mater. Des.* 208, 109900. doi:10.1016/j.matdes.2021.109900

Fan, Q., Huang, Y., Chen, M., Li, Y., Song, W., Fang, D., et al. (2019). Integrated design of component and configuration for a flexible and ultrabroadband radar absorbing composite. *Compos. Sci. Technol.* 176, 81–89. doi:10.1016/j.compscitech.2019.04.008

Fu, X., Fan, Y., Wang, J., Li, Y., Feng, M., Chen, H., et al. (2019). Ultra-wideband microwave absorber via an integrated metasurface and impedance-matching lattice design. *J. Phys. D. Appl. Phys.* 52 (31), 31LT01. doi:10.1088/1361-6463/ab2030

Hu, H., Liao, W., Hou, L., An, Q., and Zhang, X. (2021). Ultra-thin ultra-broadband metamaterial absorber based on impedance surface. *AEU - Int. J. Electron. Commun.* 138, 153860. doi:10.1016/j.aeue.2021.153860

Huang, H., Wang, W., Hua, M., Kuang, J., Ma, Y., Guo, Z., et al. (2020). Broadband radar absorbing characteristic based on periodic hollow truncated cone structure. *Phys. B Condens. Matter* 595, 412368. doi:10.1016/j.physb.2020.412368

Huang, Y., Song, W., Wang, C., Xu, Y., Wei, W., Chen, M., et al. (2018). Multi-scale design of electromagnetic composite metamaterials for broadband microwave absorption. *Compos. Sci. Technol.* 162, 206–214. doi:10.1016/j.compscitech.2018.04.028

Jing, J., Xiong, Y., Shi, S., Pei, H., Chen, Y., Lambin, P., et al. (2021). Facile fabrication of lightweight porous FDM-Printed polyethylene/graphene nanocomposites with enhanced interfacial strength for electromagnetic interference shielding. *Compos. Sci. Technol.* 207, 108732. doi:10.1016/j.compscitech.2021.108732

Kotsilkova, R., Ivanov, E., Todorov, P., Petrova, I., Volynets, N., Paddubskaya, A., et al. (2017). Mechanical and electromagnetic properties of 3D printed hot pressed nanocarbon/poly(lactic) acid thin films. *J. Appl. Phys.* 121 (6), 064105. doi:10.1063/1.4975820

Landy, N. I., Sajuyigbe, S., Mock, J. J., Smith, D. R., and Padilla, W. J. (2008). Perfect metamaterial absorber. *Phys. Rev. Lett.* 100 (20), 207402. doi:10.1103/PhysRevLett.100.207402

Lei, L., Yao, Z., Zhou, J., Wei, B., and Fan, H. (2020). 3D printing of carbon black/polypropylene composites with excellent microwave absorption performance. *Compos. Sci. Technol.* 200, 108479. doi:10.1016/j.compscitech.2020.108479

Li, Y., Chen, Q., Wu, B., Shi, L., Tang, P., Du, G., et al. (2019). Broadband perfect metamaterial absorber based on the gallium arsenide grating complex structure. *Results Phys.* 15, 102760. doi:10.1016/j.rinp.2019.102760

Liu, L., Zhang, Y., Sheng, J. Q., Wei, Y. M., Liu, R. M., Yu, W., et al. (2021). Gradient honeycomb absorber with high power handling capability. *Appl. Phys. A* 127 (2), 129. doi:10.1007/s00339-020-04223-9

Liu, W., Tian, J., Yang, R., and Pei, W. (2021). Design of a type of broadband metamaterial absorber based on metal and graphene. *Curr. Appl. Phys.* 31, 122–131. doi:10.1016/j.cap.2021.08.001

Luo, H., Chen, F., Wang, X., Dai, W., Xiong, Y., Yang, J., et al. (2019). A novel two-layer honeycomb sandwich structure absorber with high-performance microwave absorption. *Compos. Part A Appl. Sci. Manuf.* 119, 1–7. doi:10.1016/j.compositesa.2019.01.015

Luo, H., Lv, S., Liu, G., Cheng, Y., Ge, X., Wang, X., et al. (2022). Multi-interfacial magnetic carbon nanotubes encapsulated hydrangea-like NiMo/MoC/N-doped carbon composites for efficient microwave absorption. *Carbon* 196, 828–839. doi:10.1016/j.carbon.2022.05.046

Luo, H., Ma, B., Chen, F., Zhang, S., Wang, X., Xiong, Y., et al. (2022). Construction of hollow core-shelled nitrogen-doped carbon-coated yttrium aluminum garnet composites toward efficient microwave absorption. *J. Colloid Interface Sci.* 622, 181–191. doi:10.1016/j.jcis.2022.04.054

Mei, H., Yang, W., Zhao, X., Yao, L., Yao, Y., Chen, C., et al. (2021). *In-situ* growth of SiC nanowires@carbon nanotubes on 3D printed metamaterial structures to enhance electromagnetic wave absorption. *Mater. Des.* 197, 109271. doi:10.1016/j.matdes.2020.109271

Mei, H., Zhao, X., Zhou, S., Han, D., Xiao, S., Cheng, L., et al. (2019). 3D-printed oblique honeycomb Al2O3/SiCw structure for electromagnetic wave absorption. *Chem. Eng. J.* 372, 940–945. doi:10.1016/j.cej.2019.05.011

Pang, Y., Shen, Y., Li, Y., Wang, J., Xu, Z., Qu, S., et al. (2018). Water-based metamaterial absorbers for optical transparency and broadband microwave absorption. *J. Appl. Phys.* 123 (15), 155106. doi:10.1063/1.5023778

Ren, J., and Yin, J. Y. (2018). Cylindrical-water-resonator-based ultra-broadband microwave absorber. *Opt. Mat. Express* 8 (8), 2060. doi:10.1364/OME.8.002060

Shen, Z., Huang, X., Yang, H., Xiang, T., Wang, C., Yu, Z., et al. (2018). An ultra-wideband, polarization insensitive, and wide incident angle absorber based on an irregular metamaterial structure with layers of water. *J. Appl. Phys.* 123 (22), 225106. doi:10.1063/1.5024319

Sheng, J., Zhang, Y., Liu, L., Quan, B., Zhang, N., Ji, G., et al. (2019). Optimizing electromagnetic wave absorption performance: Design from microscopic bamboo carbon nanotubes to macroscopic patterns. *J. Alloys Compd.* 809, 151866. doi:10.1016/j.jallcom.2019.151866

Song, Z., Wang, Z., and Wei, M. (2019). Broadband tunable absorber for terahertz waves based on isotropic silicon metasurfaces. *Mat. Lett.* 234, 138–141. doi:10.1016/j.matlet.2018.09.084

Wang, Q., and Cheng, Y. (2020). Compact and low-frequency broadband microwave metamaterial absorber based on meander wire structure loaded resistors. *AEU - Int. J. Electron. Commun.* 120, 153198. doi:10.1016/j.aeue.2020.153198

Wang, T., Lu, X., and Wang, A. (2020). A review: 3D printing of microwave absorption ceramics. *Int. J. Appl. Ceram. Technol.* 17 (6), 2477–2491. doi:10.1111/ijac.13604

Xiao, S., Mei, H., Han, D., and Cheng, L. (2019). 3D printed SiC nanowire reinforced composites for broadband electromagnetic absorption. *Ceram. Int.* 45 (9), 11475–11483. doi:10.1016/j.ceramint.2019.03.015

Xiong, Y., Chen, F., Cheng, Y., and Luo, H. (2022). Rational design and fabrication of optically transparent broadband microwave absorber with multilayer structure based on indium tin oxide. *J. Alloys Compd.* 920, 166008. doi:10.1016/j.jallcom.2022.166008

Xu, Y., Yuan, L., Liang, Z., Wang, X., and Li, X. (2017). A wide frequency absorbing material added CIPs using the fuse deposition modeling. *J. Alloys Compd.* 704, 593–598. doi:10.1016/j.jallcom.2017.02.068

Yang, D., Yin, Y., Zhang, Z., Li, D., and Cao, Y. (2020). Wide-angle microwave absorption properties of multilayer metamaterial fabricated by 3D printing. *Mat. Lett.* 281, 128571. doi:10.1016/j.matlet.2020.128571

Yin, L., Tian, X., Shang, Z., and Li, D. (2019). Ultra-broadband metamaterial absorber with graphene composites fabricated by 3D printing. *Mat. Lett.* 239, 132–135. doi:10.1016/j.matlet.2018.12.087

Zhang, C., Ji, S., Zhao, J., Wu, H., and Dai, H. (2021a). Design and analysis of a broadband metamaterial absorber applied to visible light band. *Opt. Mat. (Amst).* 121, 111533. doi:10.1016/j.optmat.2021.111533

Zhang, H., Ling, F., Wang, H., Zhang, Y., and Zhang, B. (2020a). A water hybrid graphene metamaterial absorber with broadband absorption. *Opt. Commun.* 463, 125394. doi:10.1016/j.optcom.2020.125394

Zhang, H., Ling, F., and Zhang, B. (2021b). Broadband tunable terahertz metamaterial absorber based on vanadium dioxide and Fabry-Perot cavity. *Opt. Mat. (Amst).* 112, 110803. doi:10.1016/j.optmat.2021.110803

Zhang, Z., Zhang, L., Chen, X., Wu, Z., He, Y., Lv, Y., et al. (2020b). Broadband metamaterial absorber for low-frequency microwave absorption in the S-band and C-band. *J. Magn. Magn. Mat.* 497, 166075. doi:10.1016/j.jmmm.2019.166075

Zhou, D., Huang, X., and Du, Z. (2017a). Analysis and design of multilayered broadband radar absorbing metamaterial using the 3-D printing Technology-Based method. *IEEE Antennas Wirel. Propag. Lett.* 16, 133–136. doi:10.1109/LAWP.2016.2560904

Zhou, Q., Yin, X., Ye, F., Liu, X., Cheng, L., Zhang, L., et al. (2017b). A novel two-layer periodic stepped structure for effective broadband radar electromagnetic absorption. *Mater. Des.* 123, 46–53. doi:10.1016/j.matdes.2017.03.044